Self-Assembly of Carboranethiol Isomers on Au{111}: Intermolecular Interactions Determined by Molecular Dipole Orientations

J. Nathan Hohman,[†] Pengpeng Zhang,[†] Elizabeth I. Morin,[†] Patrick Han,[†] Moonhee Kim,[†] Adam R. Kurland,[†] Patrick D. McClanahan,[†] Viktor P. Balema,[‡] and Paul S. Weiss[†,*]

[†]Departments of Chemistry and Physics, 104 Davey Laboratory, The Pennsylvania State University, University Park, Pennsylvania 16802-6300 and [‡]Aldrich Materials Science, Sigma-Aldrich Company, 6000 North Teutonia Avenue, Milwaukee, Wisconsin 53209

ABSTRACT Self-assembled monolayer (SAM) structures and properties are dominated by two interactions: those between the substrate and adsorbate and those between the adsorbates themselves. We have fabricated self-assembled monolayers of *m*-1-carboranethiol (M1) and *m*-9-carboranethiol (M9) on Au{111}. The two isomers are nearly identical geometrically, but calculated molecular dipole moments show a sizable difference at 1.06 and 4.08 D for M1 and M9 in the gas phase, respectively. These molecules provide an opportunity to investigate the effect of different dipole moments within SAMs without altering the geometry of the assembly. Pure and co-deposited SAMs of these molecules were studied by scanning tunneling microscopy (STM). The molecules are indistinguishable in STM images, and the hexagonally close-packed adlayer structures were found to have ($\sqrt{19} \times \sqrt{19}$)*R*23.4° unit cells. Both SAMs display rotational domains without the protruding or depressed features in STM images associated with domain boundaries in other SAM systems. Differing orientations of molecular dipole moments influence SAM properties, including the stability of the SAM and the coverage of the carboranethiolate in competitive binding conditions. These properties were investigated by dynamic contact angle goniometry, Kelvin probe force microscopy, and grazing incidence Fourier transform infrared spectroscopy.

KEYWORDS: self-assembly · self-assembled monolayers · carboranethiol · contact angle · Kelvin probe · Fourier transform infrared spectroscopy · scanning tunneling microscopy · dipole moment

The design of nanoscale structures with high degrees of complexity and functionality continues to be a driving force in the field of nanoscale fabrication. Utilizing self-assembly for the control of interface chemistry is an attractive alternative to top-down fabrication for supramolecular length scales. Self-assembled monolayers of thiols on gold have been model systems for the study of self-assembly methodology.[1−10] Control over the chemical and physical properties of the interface, coupled with the ability to isolate, to probe, and to interact with individual molecules embedded in a self-assembled monolayer (SAM) matrix has enabled tailored molecular designs for directed assembly.[11−17]

The canonical *n*-alkanethiol SAM on Au{111} is one of the most widely studied self-assembled systems due to its simplicity of fabrication and availability.[18−25] The alkanethiolate monolayers on Au{111} form well-packed ($\sqrt{3} \times \sqrt{3}$)*R*30° lattices relative to the (1 × 1) unit cell of the gold substrate.[5,26] A well-ordered monolayer is formed through the interplay between the Au−S bond strength and the sum of the weaker intermolecular interactions between alkyl chains in their standing phase.[9,22,26,27]

We have explored the influence of intermolecular and geometric factors that impact SAM structure and function. In particular, we have focused on the self-assembly of amide-containing alkanethiols, which exhibit strong directional hydrogen-bonding interactions within the monolayer, and weakly interacting adamantanethiols that form labile SAMs.[12,13,28,29] Diamondoid cage structures,[29−31] conjugated,[32−35] and internally[12,13] or terminally functionalized[14,15,36−39] molecules all have been modified with thiols, generating surfaces with divergent structures and functions. Determination of the design principles that can be employed to tailor SAM structures is a critical undertaking. Altering functional groups to tailor intermolecular interactions is straightforward. However, making direct comparisons between adsorbates is complicated by the fact that introducing a new functional group alters both the internal dipole moment and the geometry of the SAM constituents simultaneously. Since both steric and electronic properties (*e.g.*, geometry and dipole) play critical roles in the behavior of SAMs, the

*Address correspondence to stm@psu.edu.

Received for review October 9, 2008 and accepted February 06, 2009.

Published online February 25, 2009.
10.1021/nn800673d CCC: $40.75

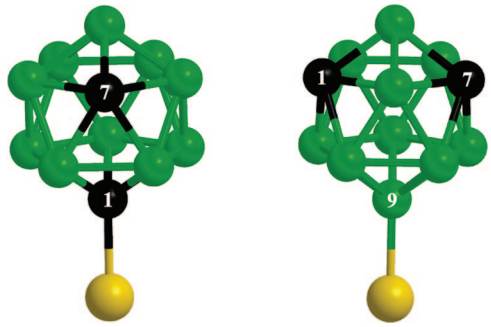

Figure 1. Two thiolated positional isomers of 1,7-dicarba-*closo*-dodecaborane *m*-1-carboranethiol (left, M1) and *m*-9-carboranethiol (right, M9). All carbon and boron atoms are hexacoordinate. Hydrogen atoms are present at each vertex but have been omitted for clarity.

ability to examine these factors independently represents an important advance.

While there are few examples in the literature of inorganic molecules used to form SAMs, one important set of exceptions, the carboranethiols, represent an elegant solution to the problem described above. The icosahedral dicarba-*closo*-dodecaboranes, having the formula $C_2B_{10}H_{12}$, have been some of the most widely studied boron cluster compounds since the first reports of their syntheses and unique structures in 1963.[40−43] These compounds have a nearly regular icosahedral boron−carbon cluster geometry with a hydrogen atom at each of the vertices. A striking characteristic of the icosahedral carborane structure is hexacoordination of the carbon and boron atoms, a feature attributed to the electron-deficient nature of boron hydrides and delocalized bonding present in the cage. The two carbon atoms in the icosahedron can be either adjacent (*ortho*-carborane), separated by a boron atom (*meta*-carborane), or at opposite ends of the icosahedron (*para*-carborane); the relative carbon atom positions influence the net molecular dipole of the cluster with *o*-carborane having the highest dipole moment and *p*-carborane having no net dipole. Thus, it is possible to alter the molecular dipole magnitude substantially without appreciably changing the molecular geometry. Further, carboranes are amenable to functionalization, including electrophilic aromatic substitution, electrophilic halogenation, alkylation, metalation, and sulfhydrylation.[44−48] Importantly, sulfhydrylation has also enabled carboranes to be used as constituents in SAMs.[49] Unlike other boron hydride compounds, the carboranes are also highly resistant to thermal and chemical degradation,[43] which allows them to undergo the processing necessary for the formation of high-quality SAMs. Due to their stability and interesting structural properties, they have also been incorporated into polymers,[50,51] dendrimers,[52] as nanocar wheels,[53] and as spacers in molecular switches.[54]

RESULTS AND DISCUSSION

Here, we report the preparation of self-assembled monolayers of two positional isomers, 1-mercapto-1,7-dicarba-*closo*-dodecaborane and 9-mercapto-1,7-dicarba-*closo*-dodecaborane; henceforth *m*-1-carboranethiol (**M1**) and *m*-9-carboranethiol (**M9**), respectively; both molecules are shown schematically in Figure 1. The **M1** and **M9** isomers have different molecular dipoles yet essentially identical geometric structures. Herein we will present our analysis of the lattice structures for the **M1** and **M9** isomers on Au{111} as determined by scanning tunneling microscopy (STM). Their identical SAM structures belie significant differences in the stabilities and chemical resistance of the monolayers, stemming from differences in their molecular dipoles. In order to visualize the orientations of the molecular dipoles, we calculate the molecular dipole moments of both isomers at the B3LYP levels and employ Kelvin probe force microscopy (KPFM) to measure the modulation of the gold work function induced by the presence of the respective SAMs. To test the influence of intermolecular dipole−dipole interactions within the SAM on its global properties, we measure the wettability of the carboranethiolate-modified surfaces by dynamic contact angle measurements and monitor the exchange of carboranethiolate SAMs with **C12** and the ratio of **M1**:**M9** in a competitive adsorption environment by grazing incidence Fourier transform infrared spectroscopy (FTIR).

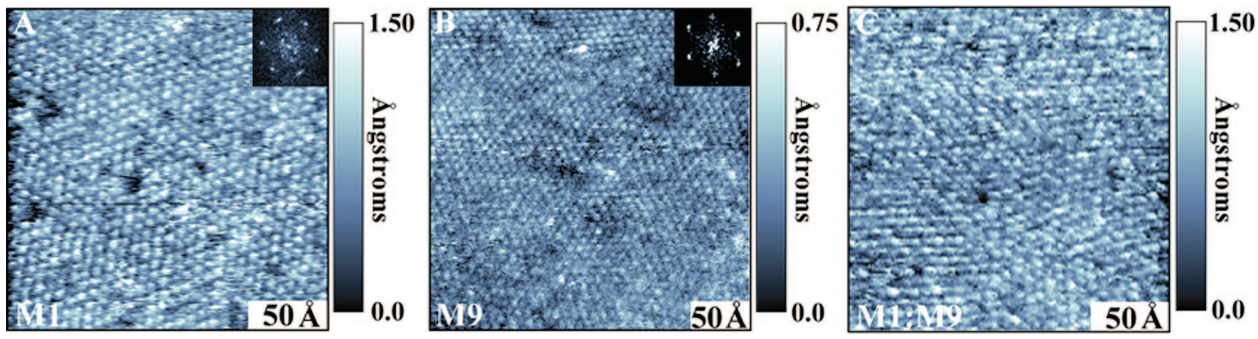

Figure 2. Scanning tunneling microscope images of SAMs of (A) M1, (B) M9, and (C) an adlayer prepared from a 1:1 M1:M9 solution, all on Au{111}. All images were collected at a sample bias of 1.0 V and a tunneling current of 3.0 pA under ambient conditions. Small depressions and protrusions in all three images are within 1 Å and are inconsistent with substrate vacancy islands. Also shown in the insets are the Fourier transforms of (A) and (B) showing reciprocal lattice points from which nearest-neighbor spacings were calculated.

Ambient STM images of molecularly resolved **M1** and **M9** SAMs (Figure 2A,B) show strong structural similarities, which are also evident in co-deposited SAMs of **M1** and **M9** at a 1:1 ratio in the solution used to deposit them (Figure 2C). All three SAMs are hexagonally close packed with sparse defects; in fact, the images depict large areas of **M1** and **M9**, respectively, for which no domain boundaries could be found. Topographically, **M1** and **M9** are indistinguishable by STM imaging since both isomers appear as round protrusions of identical apparent height. Fourier transformations of the images in Figure 2A,B yield identical nearest-neighbor spacings of 7.2 ± 0.4 Å for both **M1** and **M9**, in good agreement with the 6.97 Å equilibrium nearest-neighbor spacing in crystals of the unsubstituted carboranes.[55] Co-deposited monolayers of **M1** and **M9** also display the same nearest neighbor spacings as monolayers of the pure isomers. Changing the bias polarity has no effect on the observed images and does not differentiate between molecules in mixed carboranethiol SAMs. Since the two isomers have such similar geometries, it is not surprising that the final SAMs have identical structures, with the same measured nearest-neighbor spacings.

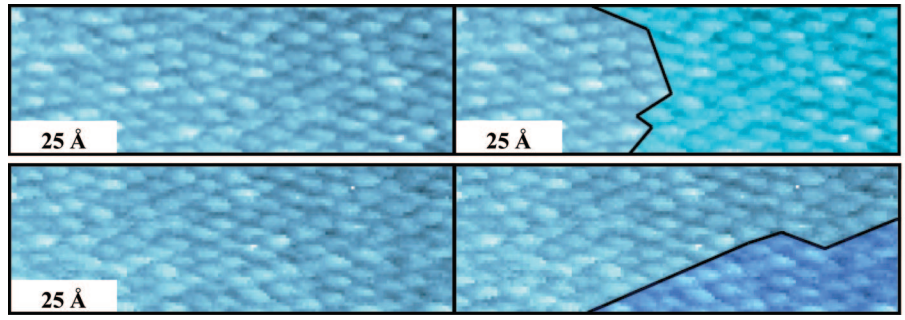

Figure 3. STM images of two characteristic rotational domain boundaries found in carboranethiolate SAMs. The molecular rows shift smoothly from one domain to the next; there are no depressed or protruding features related to the domain boundary, a feature that distinguishes carboranethiolate SAMs from those of alkanethiolate and other SAM systems. The images on the right are colorized versions of the raw images on the left to emphasize rotations of the lattice directions.

Lattice defects appear similar for both **M1** and **M9** SAMs. Most notable are small apparent depressions and protrusions of approximately 1.0 Å, neither of which appreciably affect the organization of the lattice. Both SAMs lack the prominent domain boundaries and substrate vacancy islands characteristic of *n*-alkanethiolate and diamondoid SAMs.[5,27,30] Instead, one finds rotational domain boundaries at which the directionality of molecular rows periodically shifts with no discernible change in height or spacing, as highlighted in representative STM images in Figure 3.

We considered several possibilities for a carboranethiolate SAM unit cell with nearest-neighbor spacings of 7.2 ± 0.4 Å. Possible cells include ($\sqrt{93} \times \sqrt{93}$)*R*21.05°, ($\sqrt{97} \times \sqrt{97}$)*R*15.30°, (5 × 5), and ($\sqrt{19} \times \sqrt{19}$)*R*23.4°, which have nearest-neighbor spacings of 6.94, 7.09, 7.20, and 7.25 Å, respectively. Among those, only the (5 × 5) and ($\sqrt{19} \times \sqrt{19}$)*R*23.4° unit cells form overlayers commensurate with the gold surface. While the nearest-neighbor spacing of the (5 × 5) unit cell, 7.20 Å, is in good agreement with the measured spacing of 7.2 ± 0.4 Å, the presence of rotational domains reduces the likelihood of this candidate structure. The identical measured spacings and presence of rotational domains lead us to propose a ($\sqrt{19} \times \sqrt{19}$)*R*23.4° unit cell with respect to the gold substrate as the adlayer structure. The ideal ($\sqrt{19} \times \sqrt{19}$)*R*23.4° unit cell contains three carboranethiolate molecules, has a nearest-neighbor spacing of 7.25 Å, and has a lattice constant of 12.57 Å. Our proposed structure is shown in Figure 4. There are two equivalent registrations to the Au{111} substrate for this unit cell, shown schematically in Figures 4B,C. The first bonding mode is through a mixture of atop and 3-fold hollow sites at a 1:2 ratio, while the second is through all equivalent near-bridge sites. While we consider the ($\sqrt{19} \times \sqrt{19}$)*R*23.4° unit cell to be the most likely structure, we cannot conclusively rule out the possibility of a (5 × 5) structure or competition between (5 × 5) and ($\sqrt{19} \times \sqrt{19}$)*R*23.4° unit cells.

The measured apparent height of the carboranethiolate adsorbates is estimated by comparison to the apparent height of a known adsorbate, 1-dodecanethiolate (**C12**). From the STM image of a mixed monolayer of **C12** and the carboranethiolate, a line scan is taken over phase-separated domains of **C12** and **M1** or **M9**. The average difference in apparent

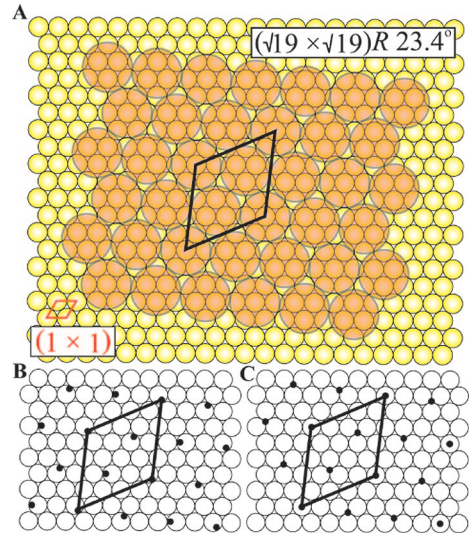

Figure 4. Proposed ($\sqrt{19} \times \sqrt{19}$)*R*23.4° unit cell for both carboranethiolate isomers and mixed monolayers is shown here (A). There are two possible registries to the gold surface, an alternating atop and 3-fold hollow configuration, shown in (A) and (C), and an all-equivalent near-bridge configuration shown in (B).

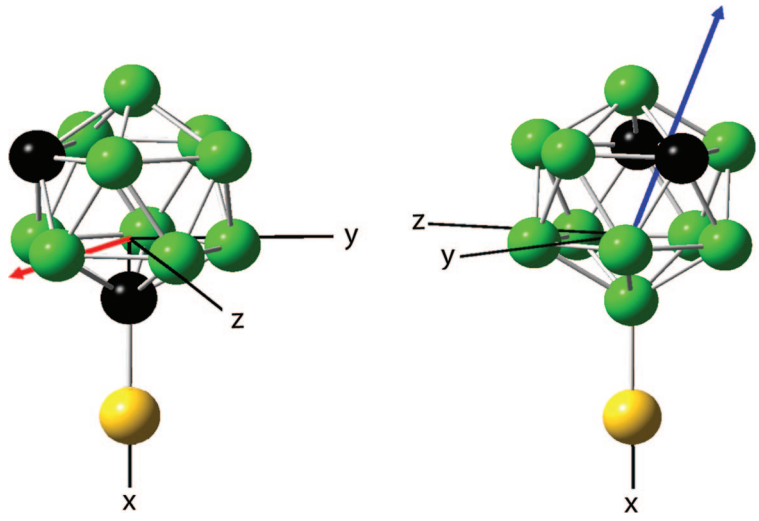

Figure 5. Calculated dipole vectors for isolated M1 (left) and M9 (right). We have adopted the convention that the arrow points in the direction of positive charge. Vectors correspond to dipole moment magnitudes of 1.06 and 4.08 D for M1 and M9, respectively. Component vectors are found in Supplemental Table 1 in the Supporting Information. All hydrogen atoms have been omitted for clarity.

height between a domain of carboranethiolate and a domain of **C12** is 2.4 ± 0.3 Å, corresponding to an apparent carboranethiolate height of 9.8 ± 0.3 Å, assuming a height of 12.2 Å for **C12**.[29,56,57] This value is a simple comparison of apparent heights and does not take into account any differences in conductivities for the carboranethiolate SAM domains as compared to the **C12** domains.

As discussed above, SAMs of both carboranethiolate isomers generate the same lattice because of their identical geometries; however, the differences in relative positions of the carbon and sulfur atoms result in important differences in the magnitudes and relative directions of the dipole moments. We evaluate their distinct properties using molecular dipole moment calculations, relative water contact angles, Kelvin probe force measurements of the work functions, and grazing incidence FTIR.

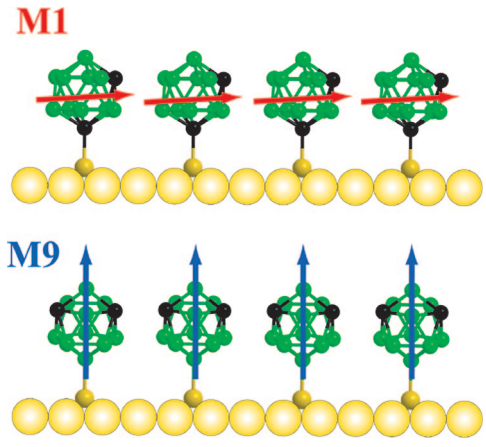

Figure 6. Schematic showing relative dipole orientations for the carboranethiolate isomers as interpreted from our calculations and from the KPFM measurements of the carboranethiolate-modified gold. The free M1 molecule (top) has lower magnitude dipoles, but they are oriented nominally parallel to the surface, while M9 (bottom) has a larger dipole moment, but they are oriented normal to the surface. The positive end of the dipole moment direction is considered to lie between the carbon atoms. We have adopted the convention that the dipole arrow points in the direction of positive charge.

The molecular dipole of unsubstituted *m*-carborane has been calculated to be 2.84 D.[57] Both the magnitude and direction of the molecular dipole with respect to the gold surface are divergent for the two substituted isomers, due to the relative electronegativities of carbon and sulfur compared to boron (2.55 and 2.58 *vs* 2.04 Pauling units,[58] respectively). The difference in charge distribution around the cage leads to a substantial difference in the acidity of the thiol proton of the free molecule, with reported pK_a values of 5.30 and 9.45 for **M1** and **M9**,[59] respectively.

Strong dipole−dipole interactions within SAMs influence adlayer structures and functions.[13,15] Thus, it is important to calculate the magnitudes and directions of the molecular dipole moments in the carboranethiol species in order to gain insight into the relative intermolecular forces within the SAM. While complete active space with second-order perturbation theory (CASPT2) and higher-level theories would provide better treatment of electron delocalization in carborane derivatives, density functional theory (DFT) has been shown to balance computation cost and efficiency for carboranes of moderate size.[57,60] Using DFT with the 6-31G basis set, we calculated the dipole moments for **M1** and **M9** in the gas phase to be 1.06 and 4.08 D, respectively. For comparison, calculations were also performed at the Hartree−Fock (HF) and MP2 levels, both with the 6-31G basis set (Supporting Information Table 1). The calculated dipole moments, shown in Figure 5, are consistent across techniques. For both molecules, the positive end of the dipole moment direction lies between the carbon atoms. The presence of positive charge at the relatively electronegative carbon atoms is attributed to charge transfer into vacant boron bonding orbitals.[57] The positive pole at the carbon atoms also explains the higher acidity of the **M1** isomer, due

TABLE 1. Comparisons between Carboranethiol SAMs

	contact angle (deg)		hysteresis (deg)
	θ_a	θ_r	Δ
m-1-carboranethiolate (**M1**)	82 ± 2	71 ± 1	11 ± 1
m-9-carboranethiolate (**M9**)	72 ± 4	52 ± 1	20 ± 4
3:1 **M1**:**M9**	82 ± 1	67 ± 1	15 ± 1
1:1 **M1**:**M9**	82 ± 2	66 ± 1	16 ± 1
1:3 **M1**:**M9**	82 ± 1	68 ± 1	14 ± 1
1-dodecanethiolate (**C12**)	107 ± 1	97 ± 1	10 ± 2

to stabilization of the negatively charged sulfur atom after deprotonation. It should be noted that the dipole calculations were performed for isolated thiol molecules in the gas phase. The interplay of effects such as chemisorption, thiol to thiolate conversion, the presence of neighboring SAM molecules, and the formation of a bond dipole will all influence the final molecular moment of molecules in a SAM. Therefore, we have not attempted to determine the absolute values of the adsorbed molecular dipoles from our Gaussian calculations alone. Nonetheless, the calculated gas-phase dipoles are valuable as a point of reference in the analysis of the different work functions of the SAM surfaces.[61,62]

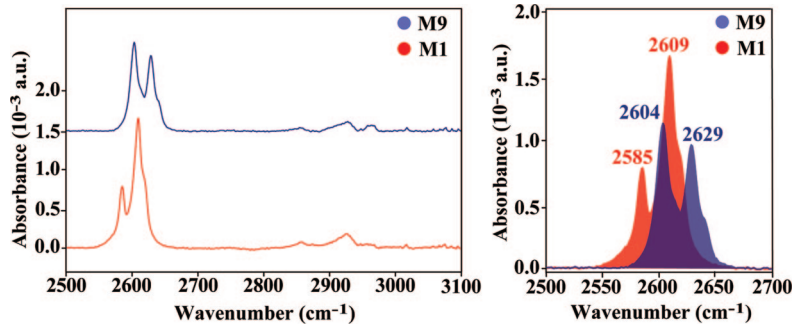

Figure 7. Grazing incidence FTIR spectra of M1 (red) and M9 (blue) on Au{111}. The spectrum between 2500 and 3100 cm^{-1} (left) is dominated by the strong absorption around 2600 cm^{-1}, corresponding to the B−H vibrations. Weak absorption in the region around 2900 cm^{-1} is most likely due to adventitious organics. The overlay (right) of the region between 2500 and 2700 cm^{-1} emphasizes the differences between the spectra of the two isomers.

We employed KPFM to measure the influence of **M1** and **M9** monolayers on the work function of the gold substrate due to their different dipole orientations. This technique does not provide absolute measurements of the final dipole moments for the molecules, but by using the calculated values as a guide, we are able to infer dipole orientations from the results.[63] We measured the modulation of the work functions of **M1**- and **M9**-coated substrates relative to that of a clean Au{111} substrate. Our results show a modest work function decrease of 90 ± 20 meV upon **M1** adsorption, whereas **M9** adsorption decreased the work function by 480 ± 20 meV. A dipole more perpendicular to the surface will have a stronger influence on the work function, while one parallel to the surface will have a weaker influence.[64,65] Additionally, if the positive pole is pointing away from the surface, the work function will decrease, while the opposite holds true if the negative pole points away.[63] The **M9** isomer possesses a larger dipole moment and is oriented nominally normal to the gold surface, with the positive pole pointing away from the substrate. The result is a much larger decrease in work function than that observed for the **M1** isomer, in which the dipole is nominally parallel to the surface.

Within the framework of this agreement between modeled dipoles and KPFM measurements, we can describe and rationalize the divergent SAM properties of the two carboranethiolate isomers. Once adsorbed on the gold surface, the molecular dipoles have a strong influence on the final SAM properties. Figure 6 illustrates a schematic of the orientation of the dipoles relative to the gold surface. The weaker dipole of **M1** is oriented relatively parallel to the surface, while the stronger dipole of **M9** is oriented relatively normal to the surface. This difference is manifest in contrasts between the properties of the SAMs, as discussed below.

Plastic crystalline phases, where component molecules are free to reorient while maintaining positional order in their lattice, have been reported in *o*- and *m*-carborane.[66] While thiolate attachment removes many orientational degrees of freedom, we do not discount the possibility that the molecules may be freely rotating, especially in the case of the **M9**, which does not possess the favorable lateral dipole−dipole interactions present in **M1**.

As would be expected, the difference in dipole magnitude and direction results in a different surface hydrophobicity, as measured by contact angle goniometry. Dynamic contact angles for 10 μL drops of 18.2 MΩ water on SAMs of **M1**, **M9**, co-deposited **M1**/**M9**, and **C12** were compared. Measurements shown in Table 1 indicate that all carboranethiol SAMs are significantly more hydrophilic than the reference alkanethiolate **C12** SAM. The larger dipole moment and strong influence on the gold work function cause **M9** to be more hydrophilic than its less-polar positional isomer, **M1**. The mixed monolayers, in all three cases, exhibited advancing contact angles (θ_a) that were close to those measured for **M1**, while receding angles (θ_r) were between those measured for the two pure carboranethiols. That the **M1** isomer continues to dominate the surface contact properties in co-deposited monolayers, even at a high relative solution concentration of the **M9** species, is surprising but is in agreement with the spectroscopic data presented below. We anticipated an intermediate value for the advancing angle. We attribute this result to incomplete understanding of the nanoscale structure of the mixed monolayers. It is unknown if the **M1** and **M9** are intermixed, form distinct, phase-separated domains, or whether the dipole of **M9** is modified by the presence of **M1**.

TABLE 2. Preference for M1 in Co-deposited SAMs

	%M1	%M9	error (n = 3)
3:1 **M1**:**M9**	89%	11%	±5%
1:1 **M1**:**M9**	70%	30%	±5%
1:3 **M1**:**M9**	56%	44%	±2%

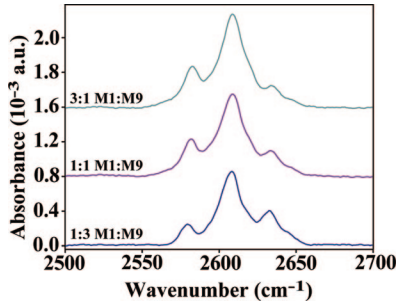

Figure 8. Grazing incidence FTIR spectra of codeposited M1 and M9 at 1:3, 1:1, and 3:1 ratios prepared such that the total concentration of carboranethiol in each case was 1 mM. The 2585 cm^{-1} peak is well-resolved and is representative of the M1 isomer. Comparisons of this peak area in a pure M1 SAM to the corresponding peak areas in the spectra of codeposited SAMs' enable estimation of M1 coverages. In all cases, the M1 dominates the surface coverage in competitive environments.

Grazing incidence FTIR spectra of **M1** and **M9** SAMs were obtained from 800 to 4000 cm^{-1}, a subset of which are shown in Figure 7A. Peaks in the region between 2500 and 2700 cm^{-1} are attributed to B−H stretches.[67] The presence of an absorption in this region is characteristic of the carboranes and is often used as a marker for these species due to the intensity of the B−H absorption and the lack of spectral interference. Figure 7B shows an overlay of the carboranethiolate SAM spectra. We observe distinct features in the B−H stretching region; both isomers display two main peaks with associated shoulders, an overlay of which is shown in Figure 7B. This IR region is generally reported to be broad and featureless in solution.[67] While it is tempting to attribute the differences in intensity and energy to nonequivalence of the B−H stretches, Leites *et al.* have observed fine structure in the B−H region for carboranes with bulky substituents and instead attributed it to correlation field splitting.[67−70]

The **M1** peak at 2585 cm^{-1} is the only well-resolved peak in a mixed monolayer and represents a spectroscopic handle for which we can design an experiment estimating relative coverage of the two isomers in a competitive assembly environment. We deposited SAMs from ethanolic solutions of **M1** and **M9** such that the total carboranethiol concentration was 1 mM at 1:3, 1:1, and 3:1 ratios; representative spectra of each are shown in Figure 8. These spectra show features of both **M1** and **M9**. The 2585 cm^{-1} peak area in coadsorbed SAMs was measured and compared to the corresponding peak area in the pure **M1** SAM to estimate the coverage of **M1** in the mixed monolayers. Similarly, we examined the peak at 2629 cm^{-1}, a peak characteristic of **M9**; however, for this peak, there is significant spectral overlap with the **M1** species peak at 2629 cm^{-1}, which causes systematic errors in favor of **M9**. This effect exists for **M1** but is of sufficiently low magnitude to be within the errors of our measurement. Calculated coverage values are compiled in Table 2. Peak-fitting and deconvolution strategies were considered, but incomplete peak assignments and unknown orientations led us to favor a simple analysis of relative peak areas. In all three cases, **M1** dominates the surface coverage. Even at a 1:3 **M1**:**M9** ratio, the SAM is still composed of approximately 56% **M1**. We understand this result by taking into account the dipole−dipole interactions between molecules in the **M1** and **M9** SAMs (see Figure 6). While the **M9** carboranethiol carries a larger dipole, it is oriented nominally perpendicular to the surface. In contrast, the dipole in the **M1** SAM is parallel to the surface and can orient in a head-to-tail fashion. We hypothesize that these favorable dipole−dipole interactions between molecules drive the tendency for **M1** to dominate the surface coverage in a competitive environment.

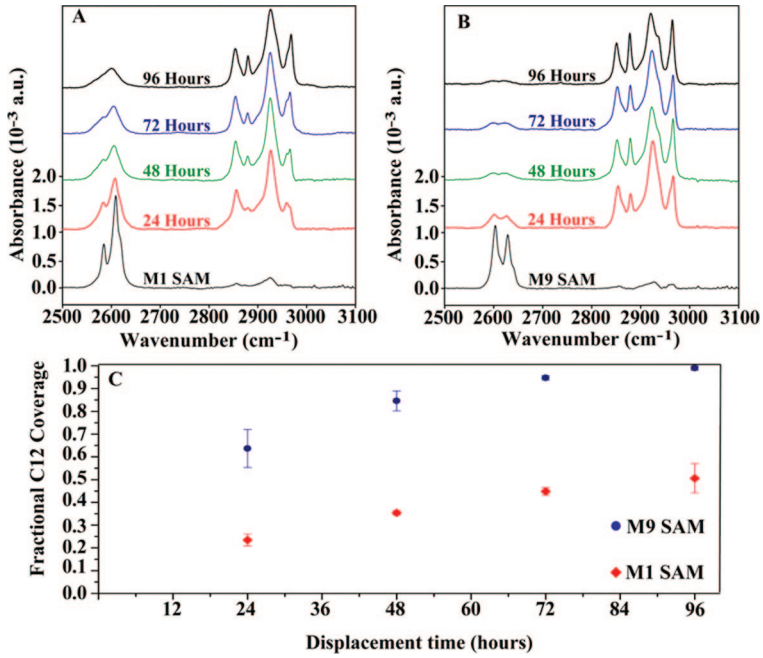

Figure 9. Spectral evolution of (A) M1 and (B) M9 SAMs during exposure to C12. Prefabricated M1 and M9 SAMs were exposed to a 1 mM ethanolic C12 solution and measured by grazing incidence FTIR at 24 h intervals (offset for clarity). B−H stretches centered around 2600 cm^{-1} decrease in intensity over the course of the reaction, with corresponding intensity increase to C−H stretches centered around 2900 cm^{-1}. Absolute C12 coverage is estimated by taking the ratio of the interval 2877 cm^{-1} peak area and the area of a SAM at full coverage. The results of 4 days of exposure are shown in C. The M1 (red) is never fully displaced by the C12, but after 4 days, the M9 (blue) displacement has approached completion. This is attributed to favorable intermolecular interactions between M1 molecules that are greatly reduced for M9.

We monitor the exchange of carboranethiolate SAMs with **C12** by STM and grazing incidence FTIR to determine the relative resistance to exchange for the two isomers. Figure 9 shows grazing incidence FTIR spectra between 2500 and 3100 cm^{-1}. Single-component **M1** and **M9** SAMs were immersed in 1 mM solutions of *n*-dodecanethiol for 24 h intervals. At the end of each interval, spectra were collected,

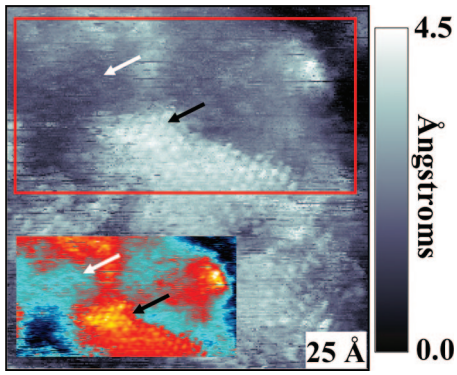

Figure 10. STM image showing M1 SAM after 48 h of exposure to a 1 mM ethanolic solution of C12. The large area scan shows patches of C12 (protruding) and domains of M1 (depressed). C12 domains are resolved with molecular resolution (black arrow). The enhanced contrast in the inset emphasizes the carboranethiolate molecules (white arrow).

and the sample was returned to solution. Over the course of 96 h, the intensity of the B−H stretches near 2600 cm^{-1} decreased, with an accompanying increase in the intensity of C−H peaks between 2800 and 3000 cm^{-1} as the coverage of aliphatic chains increased relative to the coverage of the carboranethiolate. All of the characteristic aliphatic stretches are observed, notably the CH_2 symmetric and asymmetric stretches at 2850 and 2911 cm^{-1}, the CH_3 asymmetric stretch at 2963 cm^{-1}, and the CH_3 symmetric stretch at 2877 cm^{-1}.[74] Coverage of **C12** is determined by monitoring the area of the CH_3 symmetric stretch at 2877 cm^{-1}. The area of this peak is used as an analytical marker for coverage as it is less sensitive to the orientation of the molecules than the other characteristic peaks of an alkanethiolate SAM, and there is only one methyl terminus per molecule. The results of this analysis are shown in Figure 9C. Snapshots of the exchange process were also taken using STM; an example of a partially displaced **M1** SAM is depicted in Figure 10. We observe patches of **C12** (protruding) and **M1** (less protruding).

The icosahedral cage structure of carboranethiols lends itself to direct comparison to the aliphatic cage molecule, 1-adamantanethiol (**AD**), which we have studied previously in the context of SAM displacement reactions.[10,11,28,29,71−73] These **AD** SAMs are similar in many ways to SAMs of **M1** and **M9** in terms of size, thiol attachment to the gold surface, and well-ordered hexagonal packing. In contrast to what we have found for carboranethiol SAMs, **AD** SAMs undergo rapid displacement in the presence of a solution of an *n*-alkanethiol.[29] Rapid **AD** SAM displacement is due to the availability of defect sites in which alkanethiols may insert and nucleate island growth;[28,73] islands rapidly propagate due to lower Au−S bond density and weak intermolecular forces in **AD** SAMs relative to *n*-alkanethiolate SAMs;[73] the process is driven to completion by the increased Au−S bond density and the lattice mismatch between the labile **AD** SAM and the resulting *n*-alkanethiolate SAM.[28] Considering the structural similarities of adamantanethiol to the carboranethiols, we initially expected rapid and complete displacement by *n*-alkanethiols through the same mechanism. In contrast, for **M1** and **M9**, we observe slow exchange processes. The exchange of **M9** with **C12** nearly reached completion after 4 days, significantly faster than the exchange of **M1**, but much slower than **AD**. After 4 days of exposure to **C12**, the **M1** sample surface had reached just 50% **C12** coverage. These slow rates of exchange are more akin to solution exchange of SAMs in a lattice-matched octadecanethiol system than lattice-mismatched systems like those of carboranethiolate or **AD** and **C12**.[28,29,74] We attribute this difference to the low defect density in carboranethiol SAMs, lower susceptibility of the carboranethiol to oxidation and reduction relative to alkanethiols, and stronger intermolecular interactions within the SAM. Adamantanethiolate SAMs have domain boundaries that enable substrate access from solution.[28,29,75] The tightly packed domain boundaries in **M1** and **M9** SAMs (shown in Figure 3) are inferred to be less accessible as binding sites for the displacing molecules in solution, thereby slowing the initiation of the displacement reactions. The carboranethiols are both more acidic than alkylthiols, *vide supra*, the **M1** isomer considerably so. Conjugated thiols with large molecular dipoles have been shown to generate stronger Au−S bonds than alkanethiolates, consistent with stabilizing the carboranethiolates with respect to exchange by **C12**.[76] In understanding the difference in displacement rates for **M1** and **M9**, we infer that since both molecules assume the same lattice, the difference in rates arises from interactions of dipoles in the SAMs. For the same reasons that **M1** was the preferred species in mixed monolayers, the favorable dipole−dipole interactions between **M1** molecules (with dipoles nominally parallel to the surface) stabilize the monolayer relative to exchange. The strong dipoles *normal* to the surface in **M9** SAMs do not stabilize the SAM and thus make it more susceptible to exchange than **M1**.

CONCLUSIONS AND PROSPECTS

We have characterized SAMs composed of two carboranethiol isomers, **M1** and **M9**, and found that, while they are geometrically similar, they have very different molecular dipoles. This has allowed us to separate the effects of geometry and molecular dipole. The **M1** and **M9** form hexagonally close-packed SAMs on Au{111}, assuming $(\sqrt{19} \times \sqrt{19})R23.4°$ unit cells. The work functions of the modified surfaces and calculated dipole moments for the free molecules indicate the orientations of the dipole moments—nominally normal to the surface in the case of **M9** and parallel to it in the case of **M1**. The orientations of the dipoles in the monolayers emerged as the critical variable in determining the properties of the SAM.

When designing molecules for self-assembly, the ability to tune the geometry and intermolecular interactions confers a new level of control over the system. In the case of the carboranethiols, it has led to stable monolayers with substantially different degrees of molecular exchange and behavior in competitive environments.

EXPERIMENTAL METHODS

Materials. The chemicals *m*-1-carboranethiol, *m*-9-carboranethiol, *n*-dodecanethiol, thiourea, diethyl ether, anhydrous magnesium sulfate, sodium hydroxide, silica gel (70−230 mesh), anhydrous hexanes (Sigma-Aldrich, St. Louis, MO), 1-bromododecane-d_{25} (Cambridge Isotopes, Andover, MA), and 200-proof ethanol (Pharmco, Brookfield, CT) were used as received. 1-Dodecanethiol-d_{25} was prepared as described previously.[77] All carboranethiol monolayers were fabricated by immersing flame-annealed Au{111} on mica substrates (Agilent Technology, Tempe, AZ) into gravimetrically prepared 1 mM ethanolic solutions. Perdeuterated *n*-dodecanethiolate SAMs used as background references for the normalization of FTIR spectra, as well as *n*-dodecanethiol SAMs, were prepared from 1 mM solutions overnight. After deposition from solution for 24 h, substrates were rinsed thoroughly with neat ethanol and were blown dry using ultrahigh purity argon.

STM Measurements. All STM measurements were conducted using a custom beetle-style STM under ambient conditions.[56] Piezoelectric scanner gains were calibrated using the lattice spacing of a known adsorbate, 1-dodecanethiolate on Au{111}. This lattice spacing was measured before and/or after scanning the unknown carboranethiolate SAMs. In both cases, the measured spacings of the alkanethiolate SAMs were measured in a variety of scanning directions. Carboranethiolate lattice spacings were measured from Fourier transforms of single-domain images. The vertical scale was calibrated using the monatomic step heights of the Au{111} substrate in subsequent images.

Dipole Moment Calculations. The dipole moments of isolated carboranethiol molecules in vacuum were calculated using the Gaussian 03 package and GaussView[81] on a cluster of PCs at Penn State's Materials Simulation Center. Molecular dipole moment calculations using *ab initio* density functional theory were performed for **M1** and **M9** using the 6-31G basis set. Calculations were performed at the B3LYP level, which combines the three-parameter exchange functional, developed by Becke,[78] with the Lee, Yang, and Parr correlation functional[79] and Vosko, Wilk, and Nusair local correlational functional.[80] For comparison, calculations were also performed at the Hartree−Fock (HF) and MP2 levels, both with the 6-31G basis set.[81] The detailed results are given in the Supporting Information.

Contact Angle Goniometry. Contact angle measurements were made using a custom apparatus with a CCD camera (Hitachi Denshin America, Ltd., Woodbury, NY) equipped with an InfiniStix 0.50× magnification, 94 mm focal length lens (Infinity, Boulder, CO), using a National Instruments IMAQ-PCI card (National Instruments, Austin, TX) for data acquisition. Images were captured using National Instruments Measurements and Automation software. Reproducible 5 μL droplets were deposited from a 2 mL Gilmont micrometer syringe using a blunt-tip 32 gauge needle (VWR Inc., West Chester, PA). The volume was increased to 10 μL for the advancing contact angle measurement. The drop size was increased to 20 μL and then decreased to 10 μL for the receding contact angle measurement. The contact angles were determined from images using Scion Image (Scion Corp., Frederick, MD), and each data point was an average of three measurements on each side of three static drops.

Grazing Incidence FTIR Spectroscopy. Infrared spectra were collected using a Nicolet 6700 FTIR spectrometer (Thermo Electron Corp., Waltham, MA), equipped with a liquid-nitrogen-cooled mercury−cadmium−telluride detector and a Seagull variable-angle reflection accessory (Harrick Scientific, Inc., Ossining, NY). A FTIR Purge Gas Generator (Parker-Balston, Cleveland, OH) removed water and CO_2 from the gas stream used to purge the spectrometer and its accessory. The data were collected at grazing incidence reflection (82° relative to the surface normal) with *p*-polarized light and a mirror speed of 1.27 cm/s, with a resolution of 2 cm^{-1}. All spectra were averaged over 1024 scans. Scans were normalized with spectra of perdeuterated *n*-dodecanethiolate monolayers on Au{111}.

Kelvin Probe Force Microscopy. Kelvin probe force microscope experiments were conducted on a JEOL JSPM-4500A instrument operated in ultrahigh vacuum (UHV) with a base pressure $<5 \times 10^{-10}$ Torr. The scanning probe microscope was equipped with RHK SPM 100 electronics and a PLL Pro universal AFM controller (RHK technologies, Troy, MI). A conducting Pt−Ir-coated Si cantilever (PPP-NCHPt, Nanosensors, Switzerland) was used as a KPFM probe. Prior to being loaded into the system, the probe was thoroughly rinsed with anhydrous dichloromethane and absolute ethanol to remove organic contamination from the surface and then blown dry by nitrogen gas. After loading into the UHV system, the tip was degassed at 150 °C for 2 h by radiative heating from a nearby tungsten filament. The typical spring constant and resonant frequency of the cantilever were 40 N/m and 330 kHz. The Q-factor of the cantilever in UHV was ~30 000. A clean Au{111} surface was measured before and after characterization of each SAM-modified surface to ensure that the tip condition was the same.

Acknowledgment. We gratefully acknowledge the National Science Foundation funded Center for Nanoscale Science and Penn State's National Nanotechnology Infrastructure Network for their support of this work, and Penn State's Materials Simulation Center for access to the Lion-XL supercomputer cluster. Additionally, we thank Shelley A. Claridge and Jorge Sofo for helpful discussions.

Conflict of interest: V.P.B. declares that he is an employee of Sigma-Aldrich, which sells these carboranethiols through their catalogue.

Note added after ASAP publication: In the version published online February 25, 2009, the lower left panel of Figure 3 was incorrect. The corrected figure was replaced and the paper reposted March 6, 2009.

Supporting Information Available: Computational details of the dipole moment calculations for **M1** and **M9**, including component vectors of the dipole calculated dipole moments, atomic positions in Cartesian coordinates, and the charge distribution at each atomic position. This material is available free of charge *via* the Internet at http://pubs.acs.org.

REFERENCES AND NOTES

1. Dubois, L. H.; Nuzzo, R. G. Synthesis, Structure, and Properties of Model Organic-Surfaces. *Annu. Rev. Phys. Chem.* **1992**, *43*, 437–463.
2. Dubois, L. H.; Zegarski, B. R.; Nuzzo, R. G. The Chemisorption of Organosulfur Compounds on Gold Surfaces. Construction of Well-Defined Organic-Solids. *J. Vac. Sci. Technol., A* **1987**, *5*, 634–635.
3. Laibinis, P. E.; Nuzzo, R. G.; Whitesides, G. M. Structure of Monolayers Formed by Coadsorption of 2 *Normal*-Alkanethiols of Different Chain Lengths on Gold and Its Relation to Wetting. *J. Phys. Chem.* **1992**, *96*, 5097–5105.
4. Nuzzo, R. G.; Zegarski, B. R.; Dubois, L. H. Fundamental Studies of the Chemisorption of Organosulfur Compounds on Au(111). Implications for Molecular Self-Assembly on Gold Surfaces. *J. Am. Chem. Soc.* **1987**, *109*, 733–740.
5. Poirier, G. E. Characterization of Organosulfur Molecular Monolayers on Au(111) Using Scanning Tunneling Microscopy. *Chem. Rev.* **1997**, *97*, 1117–1127.

6. Poirier, G. E.; Tarlov, M. J. The *c*(4 × 2) Superlattice of *n*-Alkanethiol Monolayers Self-Assembled on Au(111). *Langmuir* **1994**, *10*, 2853–2856.
7. Poirier, G. E.; Tarlov, M. J.; Rushmeier, H. E. 2-Dimensional Liquid-Phase and the $p \times \sqrt{3}$-Phase of Alkanethiol Self-Assembled Monolayers on Au(111). *Langmuir* **1994**, *10*, 3383–3386.
8. Ulman, A.; Eilers, J. E.; Tillman, N. Packing and Molecular-Orientation of Alkanethiol Monolayers on Gold Surfaces. *Langmuir* **1989**, *5*, 1147–1152.
9. Ulman, A. Formation and Structure of Self-Assembled Monolayers. *Chem. Rev.* **1996**, *96*, 1533–1554.
10. Mullen, T. J.; Srinivasan, C.; Shuster, M. J.; Horn, M. W.; Andrews, A. M.; Weiss, P. S. Hybrid Approaches to Nanometer-Scale Patterning: Exploiting Tailored Intermolecular Interactions. *J. Nanopart. Res.* **2008**, *10*, 1231–1240.
11. Mullen, T. J.; Dameron, A. A.; Andrews, A. M.; Weiss, P. S. Selecting and Driving Monolayer Structures through Tailored Intermolecular Interactions. *Aldrichimica Acta* **2007**, *40*, 21–31.
12. Lewis, P. A.; Smith, R. K.; Kelly, K. F.; Bumm, L. A.; Reed, S. M.; Clegg, R. S.; Gunderson, J. D.; Hutchison, J. E.; Weiss, P. S. The Role of Buried Hydrogen Bonds in Self-Assembled Mixed Composition Thiols on Au{111}. *J. Phys. Chem. B* **2001**, *105*, 10630–10636.
13. Smith, R. K.; Reed, S. M.; Lewis, P. A.; Monnell, J. D.; Clegg, R. S.; Kelly, K. F.; Bumm, L. A.; Hutchison, J. E.; Weiss, P. S. Phase Separation within a Binary Self-Assembled Monolayer on Au{111} Driven by an Amide-Containing Alkanethiol. *J. Phys. Chem. B* **2001**, *105*, 1119–1122.
14. Stranick, S. J.; Atre, S. V.; Parikh, A. N.; Wood, M. C.; Allara, D. L.; Winograd, N.; Weiss, P. S. Nanometer-Scale Phase Separation in Mixed Composition Self-Assembled Monolayers. *Nanotechnology* **1996**, *7*, 438–442.
15. Stranick, S. J.; Parikh, A. N.; Tao, Y. T.; Allara, D. L.; Weiss, P. S. Phase-Separation of Mixed-Composition Self-Assembled Monolayers into Nanometer-Scale Molecular Domains. *J. Phys. Chem.* **1994**, *98*, 7636–7646.
16. Li, Y. B.; Ma, Z.; Qi, G. C.; Yang, Y. L.; Zeng, Q. D.; Fan, X. L.; Wang, C.; Huang, W. Solvent Effects on Supramolecular Networks Formed by Racemic Star-Shaped Oligofluorene Studied by Scanning Tunneling Microscopy. *J. Phys. Chem. C* **2008**, *112*, 8649–8653.
17. Evans, S. D.; Urankar, E.; Ulman, A.; Ferris, N. Self-Assembled Monolayers of Alkanethiols Containing a Polar Aromatic Group: Effects of the Dipole Position on Molecular Packing, Orientation, and Surface Wetting Properties. *J. Am. Chem. Soc.* **1991**, *113*, 4121–4131.
18. Nuzzo, R. G.; Korenic, E. M.; Dubois, L. H. Studies of the Temperature-Dependent Phase-Behavior of Long-Chain Normal-Alkyl Thiol Monolayers on Gold. *J. Chem. Phys.* **1990**, *93*, 767–773.
19. Ulman, A.; Evans, S. D.; Snyder, R. G. Self-Assembled Monolayers of Alkanethiols on Gold: Sulfone Groups Enhancing 2-Dimensional Organization. *Thin Solid Films* **1992**, *210*, 806–809.
20. Edinger, K.; Golzhauser, A.; Demota, K.; Woll, C.; Grunze, M. Formation of Self-Assembled Monolayers of *n*-Alkanethiols on Gold: A Scanning Tunneling Microscopy Study on the Modification of Substrate Morphology. *Langmuir* **1993**, *9*, 4–8.
21. Kobayashi, K.; Umemura, J.; Horiuchi, T.; Yamada, H.; Matsushige, K. Structural Study on Self-Assembled Monolayers of Alkanedithiol Molecules. *Jpn. J. Appl. Phys. 2* **1998**, *37*, 297–299.
22. Poirier, G. E.; Pylant, E. D. The Self-Assembly Mechanism of Alkanethiols on Au(111). *Science* **1996**, *272*, 1145–1148.
23. Noh, J.; Araki, T.; Nakajima, K.; Hara, M. Molecular Decomposition *via* Striped Phase in Self-Assembled Monolayers of Alkanethiols Adsorbed on Au(111). *Mol. Cryst. Liq. Cryst.* **2001**, *371*, 95–98.
24. Ogawa, H.; Takamura, T.; Shimoyama, Y. Self-Assembly Process of Alkanethiol Monolayers. *Jpn. J. Appl. Phys. 2* **1999**, *38*, 6019–6023.
25. Bent, S. F. Heads or Tails: Which is More Important in Molecular Self-Assembly? *ACS Nano* **2007**, *1*, 10–12.
26. Noh, J.; Hara, M. Final Phase of Alkanethiol Self-Assembled Monolayers on Au(111). *Langmuir* **2002**, *18*, 1953–1956.
27. Delamarche, E.; Michel, B. Structure and Stability of Self-Assembled Monolayers. *Thin Solid Films* **1996**, *273*, 54–60.
28. Saavedra, H. M.; Barbu, C. M.; Dameron, A. A.; Mullen, T. J.; Crespi, V. H.; Weiss, P. S. 1-Adamantanethiolate Monolayer Displacement Kinetics Follow a Universal Form. *J. Am. Chem. Soc.* **2007**, *129*, 10741–10746.
29. Dameron, A. A.; Charles, L. F.; Weiss, P. S. Structures and Displacement of 1-Adamantanethiol Self-Assembled Monolayers on Au{111}. *J. Am. Chem. Soc.* **2005**, *127*, 8697–8704.
30. Fujii, S.; Akiba, U.; Fujihira, M. Geometry for Self-Assembling of Spherical Hydrocarbon Cages with Methane Thiolates on Au(111). *J. Am. Chem. Soc.* **2002**, *124*, 13629–13635.
31. Willey, T. M.; Fabbri, J. D.; Lee, J. R. I.; Schreiner, P. R.; Fokin, A. A.; Tkachenko, B. A.; Fokina, N. A.; Dahl, J. E. P.; Carlson, R. M. K.; Vance, A. L.; et al. Near-Edge X-ray Absorption Fine Structure Spectroscopy of Diamondoid Thiol Monolayers on Gold. *J. Am. Chem. Soc.* **2008**, *130*, 10536–10544.
32. Wan, L. J.; Terashima, M.; Noda, H.; Osawa, M. Molecular Orientation and Ordered Structure of Benzenethiol Adsorbed on Gold(111). *J. Phys. Chem. B* **2000**, *104*, 3563–3569.
33. Yang, G. H.; Qian, Y. L.; Engtrakul, C.; Sita, L. R.; Liu, G. Y. Arenethiols Form Ordered and Incommensurate Self-Assembled Monolayers on Au(111) Surfaces. *J. Phys. Chem. B* **2000**, *104*, 9059–9062.
34. Ishida, T.; Mizutani, W.; Choi, N.; Akiba, U.; Fujihira, M.; Tokumoto, H. Structural Effects on Electrical Conduction of Conjugated Molecules Studied by Scanning Tunneling Microscopy. *J. Phys. Chem. B* **2000**, *104*, 11680–11688.
35. Dhirani, A. A.; Zehner, R. W.; Hsung, R. P.; Guyot-Sionnest, P.; Sita, L. R. Self-Assembly of Conjugated Molecular Rods: A High-Resolution STM Study. *J. Am. Chem. Soc.* **1996**, *118*, 3319–3320.
36. Arnold, R.; Azzam, W.; Terfort, A.; Woll, C. Preparation, Modification, and Crystallinity of Aliphatic and Aromatic Carboxylic Acid Terminated Self-Assembled Monolayers. *Langmuir* **2002**, *18*, 3980–3992.
37. Wang, H.; Chen, S. F.; Li, L. Y.; Jiang, S. Y. Improved Method for the Preparation of Carboxylic Acid and Amine Terminated Self-Assembled Monolayers of Alkanethiolates. *Langmuir* **2005**, *21*, 2633–2636.
38. Collman, J. P.; Devaraj, N. K.; Eberspacher, T. P. A.; Chidsey, C. E. D. Mixed Azide-Terminated Monolayers: A Platform for Modifying Electrode Surfaces. *Langmuir* **2006**, *22*, 2457–2464.
39. Lee, J. K.; Chi, Y. S.; Choi, I. S. Reactivity of Acetylenyl-Terminated Self-Assembled Monolayers on Gold: Triazole Formation. *Langmuir* **2004**, *20*, 3844–3847.
40. Heying, T. L.; Clark, S. L.; Hillman, M.; Goldstein, H. L.; Polak, R. J.; Mangold, D. J.; Szymansk, J. W.; Ager, J. W. A New Series of Organoboranes.1. Carboranes from Reaction of Decaborane with Acetylenic Compounds. *Inorg. Chem.* **1963**, *2*, 1089–1092.
41. Fein, M. M.; Cohen, M. S.; Mayes, N.; Schwartz, N.; Bobinski, J. Carboranes. I. Preparation and Chemistry of 1-Isopropenylcarborane and its Derivatives (a New Family of Stable Clovoboranes). *Inorg. Chem.* **1963**, *2*, 1111–1115.
42. Zakharkin, L. I.; Stanko, V. I.; Brattsev, V. A.; Chapovsky, Y. A.; Ponomarenko, A. A.; Okhlobystin, O. Y.; Klimova, A. I. Synthesis + Properties of New Class of Organoboron Compounds $B_{10}C_2H_{12}$ (Baren) + Its Derivatives. *Dokl. Akad. Nauk SSSR* **1964**, *155*, 1119–1122.
43. Grimes, R. N. *Carboranes*; Academic Press: New York, 1970.
44. Plesek, J.; Hermanek, S. Sulfhydrylation of Icosahedral Carboranes. *Chem. Ind.* **1977**, 360.
45. Bregadze, V. I.; Kampel, V. T.; Godovikov, N. N. Mercuration of *ortho*-Carboranes and *meta*-Carboranes. *J. Organomet. Chem.* **1976**, *112*, 249–251.

46. Bregadze, V. I.; Usiatinsky, A. Y.; Godovikov, N. N. Thallation of Carboranes. *J. Organomet. Chem.* **1985**, *292*, 75–80.
47. Rys, E. G.; Balema, V. P.; Godovikov, N. N. Reactions of *ortho*-Carborane and *meta*-Carborane with Elemental Sulfur. *Bull. Acad. Sci. USSR, Div. Chem. Sci.* **1987**, *36*, 2227.
48. Godovikov, N. N.; Balema, V. P.; Rys, E. G. Carborane-Containing Organophosphorus Compounds. Methods of Synthesis and Properties. *Russ. Chem. Rev.* **1997**, *66*, 1017–1032.
49. Baše, T.; Bastl, Z.; Plzák, Z.; Grygar, T.; Plešek, J.; Carr, M. J.; Malina, V.; Subrt, J.; Boháček, J.; Večerníková, E. Carboranethiol-Modified Gold Surfaces. A Study and Comparison of Modified Cluster and Flat Surfaces. *Langmuir* **2005**, *21*, 7776–7785.
50. Mayes, N.; Green, J.; Cohen, M. S. Carborane Polymers. IV. Polysiloxanes. *J. Polym. Sci., Part A* **1967**, *5*, 365–379.
51. Papetti, S.; Schaeffe, B. B.; Gray, A. P.; Heying, T. L. A New Series of Organoboranes. VII. The Preparation of Poly-*m*-Carboranylenesiloxanes. *J. Polym. Sci., Part A* **1966**, *4*, 1623–1636.
52. Galie, K. M.; Mollard, A.; Zharov, I. Polyester-Based Carborane-Containing Dendrons. *Inorg. Chem.* **2006**, *45*, 7815–7820.
53. Morin, J. F.; Sasaki, T.; Shirai, Y.; Guerrero, J. M.; Tour, J. M. Synthetic Routes toward Carborane-Wheeled Nanocars. *J. Org. Chem.* **2007**, *72*, 9481–9490.
54. Ito, M.; Wei, T. X.; Chen, P. L.; Akiyama, H.; Matsumoto, M.; Tamada, K.; Yamamoto, Y. A Novel Method for Creation of Free Volume in a One-Component Self-Assembled Monolayer. Dramatic Size Effect of para-Carborane. *J. Mater. Chem.* **2005**, *15*, 478–483.
55. Baughman, R. H. NMR, Calorimetric, and Diffraction Study of Molecular Motion in Crystalline Carboranes. *J. Chem. Phys.* **1970**, *53*, 3781–3789.
56. Bumm, L. A.; Arnold, J. J.; Charles, L. F.; Dunbar, T. D.; Allara, D. L.; Weiss, P. S. Directed Self-Assembly to Create Molecular Terraces with Molecularly Sharp Boundaries in Organic Monolayers. *J. Am. Chem. Soc.* **1999**, *121*, 8017–8021.
57. Salam, A.; Deleuze, M. S.; Francois, J. P. Computational Study of the Structural and Vibrational Properties of Ten and Twelve Vertex *closo*-Carboranes. *Chem. Phys.* **2003**, *286*, 45–61.
58. Allred, A. L. Electronegativity Values from Thermochemical Data. *J. Inorg. Nucl. Chem.* **1961**, *17*, 215–221.
59. Plesek, J.; Hermanek, S.; Stibr, B. Electron-Transfer Phenomena in Isolated Icosahedral Borane Units. *J. Less Common Met.* **1979**, *67*, 225–228.
60. Knyazev, S. P.; Gordeev, E. G.; Chernyshev, E. A. Structure and Properties of 1,2-, 1,7-, and 1,12-Dicarba-*closo*-dodecaboranes(12): A Quantum Chemical Study. *Russ. Chem. Bull.* **2006**, *55*, 2154–2160.
61. Lewis, P. A.; Inman, C. E.; Yao, Y.; Tour, J. M.; Hutchison, J. E.; Weiss, P. S. Mediating Stochastic Switching of Single Molecules Using Chemical Functionality. *J. Am. Chem. Soc.* **2004**, *126*, 12214–12215.
62. Lewis, P. A.; Inman, C. E.; Maya, F.; Tour, J. M.; Hutchison, J. E.; Weiss, P. S. Molecular Engineering of the Polarity and Interactions of Molecular Electronic Switches. *J. Am. Chem. Soc.* **2005**, *127*, 17421–17426.
63. Crispin, X.; Geskin, V.; Crispin, A.; Cornil, J.; Lazzaroni, R.; Salaneck, W. R.; Bredas, J. L. Characterization of the Interface Dipole at Organic/Metal Interfaces. *J. Am. Chem. Soc.* **2002**, *124*, 8131–8141.
64. Zehner, R. W.; Parsons, B. F.; Hsung, R. P.; Sita, L. R. Tuning the Work Function of Gold with Self-Assembled Monolayers Derived from X-[C_6H_4-C C-](N)C_6H_4-SH (N = 0, 1, 2; X = H, F, CH_3, CF_3, and OCH_3. *Langmuir* **1999**, *15*, 1121–1127.
65. Ishii, H.; Sugiyama, K.; Ito, E.; Seki, K. Energy Level Alignment and Interfacial Electronic Structures at Organic Metal and Organic Organic Interfaces. *Adv. Mater.* **1999**, *11*, 605–625.
66. Brand, R.; Lunkenheimer, P.; Loidl, A. Relaxation Dynamics in Plastic Crystals. *J. Chem. Phys.* **2002**, *116*, 10386–10401.
67. Leites, L. A. Vibrational Spectroscopy of Carboranes and Parent Boranes and Its Capabilities in Carborane Chemistry. *Chem. Rev.* **1992**, *92*, 279–323.
68. Leites, L. A.; Ogorodni, N. A.; Zakharki, L. I. Structure of Decahalo-*o*-Carborane Adducts with Me_2SO and Me_2NCHO. A New Class of Compounds Capable of Hydrogen Bonding. *J. Organomet. Chem.* **1968**, *15*, 287.
69. Leites, L. A.; Vinogradova, L. E.; Aleksanyan, V. T.; Bukalov, S. S. Vibrational-Spectra of *ortho*-Carboranes, *meta*-Carboranes and *para*-Carboranes $B_{10}H_{10}C_2H_2$ and Their B-Decachloro-Substitution Products. *Bull. Acad. Sci. USSR, Div. Chem. Sci.* **1976**, *25*, 2311–2317.
70. Zakharkin, L.; Grebenni, A.; Vinograd, L.; Leites, L. A. Investigation of Reactions of 1-Halomethylcarboranes with Magnesium. *J. Gen. Chem. USSR* **1968**, *38*, 1008.
71. Dameron, A. A.; Hampton, J. R.; Smith, R. K.; Mullen, T. J.; Gillmor, S. D.; Weiss, P. S. Microdisplacement Printing. *Nano Lett.* **2005**, *5*, 1834–1837.
72. Dameron, A. A.; Hampton, J. R.; Gillmor, S. D.; Hohman, J. N.; Weiss, P. S. Enhanced Molecular Patterning *via* Microdisplacement Printing. *J. Vac. Sci. Technol., B* **2006**, *23*, 2929–2932.
73. Dameron, A. A.; Mullen, T. J.; Hengstebeck, R. W.; Saavedra, H. M.; Weiss, P. S. Origins of Displacement in 1-Adamantanethiolate Self-Assembled Monolayers. *J. Phys. Chem. C* **2007**, *111*, 6747–6752.
74. Schlenoff, J. B.; Li, M.; Ly, H. Stability and Self-Exchange in Alkanethiol Monolayers. *J. Am. Chem. Soc.* **1995**, *117*, 12528–12536.
75. Dameron, A. A.; Ciszek, J. W.; Tour, J. M.; Weiss, P. S. Effects of Hindered Internal Rotation on Packing and Conductance of Self-Assembled Monolayers. *J. Phys. Chem. B* **2004**, *108*, 16761–16767.
76. Liao, S.; Shnidman, Y.; Ulman, A. Adsorption Kinetics of Rigid 4-Mercaptobiphenyls on Gold. *J. Am. Chem. Soc.* **2000**, *122*, 3688–3694.
77. Laibinis, P. E.; Whitesides, G. M.; Allara, D. L.; Tao, Y. T.; Parikh, A. N.; Nuzzo, R. G. Comparison of the Structures and Wetting Properties of Self-Assembled Monolayers of n-Alkanethiols on the Coinage Metal Surfaces, Copper, Silver, and Gold. *J. Am. Chem. Soc.* **1991**, *113*, 7152–7167.
78. Becke, A. D. Correlation-Energy of an Inhomogeneous Electron-Gas: A Coordinate-Space Model. *J. Chem. Phys.* **1988**, *88*, 1053–1062.
79. Lee, C. T.; Yang, W. T.; Parr, R. G. Development of the Colle-Salvetti Correlation-Energy Formula into a Functional of the Electron-Density. *Phys. Rev. B* **1988**, *37*, 785–789.
80. Vosko, S. H.; Wilk, L.; Nusair, M. Accurate Spin-Dependent Electron Liquid Correlation Energies for Local Spin-Density Calculations: A Critical Analysis. *Can. J. Phys.* **1980**, *58*, 1200–1211.
81. Frisch, M. J.; Trucks, G. W.; Schlegel, H. B.; Scuseria, G. E.; Robb, M. A.; Cheeseman, J. R.; Montgomery, J. A., Jr.; Vreven, T.; Kudin, K. N. Burant, J. C.; *et al.* Gaussian 03, version 6.0; Gaussian Inc.: Wallingford, CT, 2003.